Available online at www.sciencedirect.com
ScienceDirect
International Journal of Heat and Fluid Flow 28 (2007) 1003–1012
International Journal of HEAT AND FLUID FLOW
www.elsevier.com/locate/ijhff

Heat transfer enhancement in oscillatory flow in channel with periodically upper and lower walls mounted obstacles

Abdelkader Korichi [a,1], Lounes Oufer [b,*]

[a] Centre Universitaire de Médéa, Quartier Ain D'heb, Médéa 26000, Algeria
[b] Université des Sciences et de la Technologie Houari Boumediene, Faculté de Génie Mécanique et de Génie des Procédés, Département de Génie Chimique et de Cryogénie, Laboratoire des Phénomènes de Transfert, BP 32, El-Alia, Bab-Ezzouar, Alger, Algeria

Received 21 June 2006; received in revised form 16 October 2006; accepted 1 November 2006
Available online 14 December 2006

Abstract

A numerical investigation is conducted in a rectangular channel with heated obstacles mounted alternatively on the upper and lower walls. Time-dependent two dimensional laminar flow with constant thermophysical properties is assumed for air at three values of the *Reynolds* number (50, 500 and 1000). A detailed analysis is carried out to investigate flow pattern and *Nusselt* number. Streamwise periodic contraction–expansion of the cross-section induces bifurcation from steady to unsteady flow. In the unsteady state, a self-sustained periodic oscillatory flow occurs. It is also found that a travelling wave generated by the vortex shedding contributes mainly to heat transfer enhancement.

Keywords: Heated obstacle; Heat transfer enhancement; Oscillatory flow

1. Introduction

Heat transfer enhancement in a single phase at low and moderate *Reynolds* number has been a major subject of intensive research over the years. It has numerous applications such as cooling of electronic systems, internal cooling inside turbine blades, compact heat exchangers, biomedical devices, etc. Many techniques based on both active and passive methods have been proposed to enhance heat transfer in these applications. Among these methods one can find systems involving vortex generators such as fins, ribs and other cylinders. The geometrical characteristics of vortex generators play a significant role in the rate of heat transfer. Disturbance promoters increase fluid mixing and interrupt the development of the thermal boundary layer, leading to enhancement of heat transfer. However, the complex flow characterized by the onset of successive separations, recirculation, reattachment and deflection of the flow make comprehension of the flow behaviour and heat transfer evolution in such systems more difficult.

Several investigators have studied heat transfer enhancement from surface mounted heated blocks. Sultan (2000) carried out an experimental study on the effect on heat transfer enhancement of perforated holes. He found that the mean heat transfer coefficient was enhanced up to 33.15%. The same technique was used by Leung et al. (1999) for *Reynolds* number ranging from 500 to 19,000. The authors showed an increase of up to 130% in heat transfer. Wu and Perng (1999) investigated the effect of installing an oblique plate on heat transfer over an array of five obstacles mounted in a horizontal channel and observed an enhancement of heat transfer of up to 39.5% in the value of *Nusselt* number. Jurban et al. (1996) looked at the convective heat transfer and pressure drop over an array of monocubical obstacles of both rectangular and squared shapes. Their results showed that the use of individual rectangular modules enhanced heat transfer more

* Corresponding author. Tel./fax: +213 21 24 71 69.
E-mail addresses: a_korichi@hotmail.com (A. Korichi), lounesoufer@yahoo.com (L. Oufer).
[1] Tel./fax: +213 25 58 28 10.

0142-727X/$ - see front matter © 2006 Published by Elsevier Inc.
doi:10.1016/j.ijheatfluidflow.2006.11.002

Nomenclature

A	dimensionless surface area
f	friction factor ($=4\beta H/\rho u_m^2$)
h	dimensionless obstacle height ($=h^*/H$)
H	channel height
k	thermal conductivity
L	dimensionless obstacle spacing ($=L^*/H$)
Nu	*Nusselt* number
Nu_{face}	mean face *Nusselt* number
Nu_{overall}	overall obstacle *Nusselt* number
Nu_x	local *Nusselt* number
p	dimensionless pressure
Pe	*Peclet* number
Pr	*Prandtl* number
Re	*Reynolds* number
T	temperature
t	time
u	dimensionless x-velocity component
u_m	mean velocity ($=\frac{1}{H}\int_0^H u\,dy$)
v	dimensionless y-velocity component
w	dimensionless obstacle width ($=w^*/H$)
x, y	dimensionless coordinates

Greek symbols

α	thermal diffusivity
β	linear part in pressure function of Eq. (10)
Δ	difference
θ	dimensionless temperature
ν	kinematic viscosity
ρ	density
τ	dimensionless time

Subscripts

b	bulk
f	fluid
m	mean
p	refers to one period
s	solid
w	wall
0	at inlet conditions

Superscript

*	dimensional

Other

—	time average

than did the square modules. Implementation of cylindrical modules in the middle of an array was also found to enhance heat transfer quite sensibly. In addition, the large size modules were found to increase pressure drop thoroughly. Garimella and Eibeck (1990) experimentally investigated the effect of prostration of a vortex generator on heat transfer from an array of discrete heat sources. A maximum heat transfer enhancement of about 40% was reported. Meinders and Hanjalic' (2002) presented an investigation on the effect of arrangement type of two wall-mounted cubes exposed to turbulent flow. Their results showed a large variation in the distribution of the local convective heat transfer for the various in-line and staggered configurations utilized. However, the cube-averaged heat transfer coefficients were found to be independent of the relative placement of the two cubes. In a study by Herman and Kang (2000), the effect of placement of curved vanes in a grooved channel was investigated. Enhancement of heat transfer was attained with rates comparable to those obtained in turbulent flow although at low *Reynolds* numbers. This enhancement of heat transfer was mainly the result of fluid flow acceleration between the vane and the heated block and the elimination of large recirculation regions within the grooves.

Fu and Tong (2004) carried out a numerical simulation on the effect of a oscillating cylinder on the heat transfer from heated blocks in a channel flow. Their results showed that heat transfer was remarkably enhanced as the oscillating frequency of the cylinder was in the lock-in region. Ko and Anand (2003) reported an experimental investigation of heat transfer and pressure drop in a uniformly heated rectangular channel with wall mounted porous baffles. Their findings showed that the use of such material could enhance heat transfer rates by up to 300% when compared to smooth heated channels. However, this heat transfer enhancement was accompanied by a significant increase in pressure drop. Furthermore, Sara et al. (2001a) studied the effect of block arrangement on both heat transfer and pressure drop. The results showed that the heat transfer could be enhanced or reduced depending on the spacing between blocks. The transverse blocks were found to increase the friction factor up to 30 times that of the smooth surface whereas the parallel blocks did not yield any such significant increase. In two other studies, Sara et al. (2001b, 2000) reported heat transfer and corresponding pressure drop analyses in channel with perforated rectangular cross-sectional blocks attached to its surface. They found that perforated blocks lead to enhancement of heat transfer and higher reduction in the pressure when compared to the solid blocks. Later, Sara (2003) presented an analysis of heat transfer, friction characteristics and performance analysis of convective heat transfer through a rect-

angular channel with square cross-section pin fins. His experimental results showed that the use of this technique could result in good heat transfer enhancement.

Bilen and Yapici (2001) and Bilen et al. (2001) carried out experimental investigations on the effect of orientation angle and geometrical position of wall mounted rectangular blocks. Their results indicated that the most efficient parameters were the *Reynolds* number and orientation angle. The maximum heat transfer rate was obtained at 45° orientation angle value. A numerical investigation of flow stability and heat transfer in a channel with grooved parts expansion–contraction of the two walls was carried out by Adachi and Uehara (2001). The authors found that the flow becomes unstable in the 1000–1100 *Reynolds* number range and heat transfer significantly enhanced after the bifurcation with an increase in the pressure drop for which a new correlation was established. Mixed convection from surface mounted heat sources in a duct with baffles was studied by Tsay et al. (2003). Their findings showed that an enhancement of heat transfer of up to 320% was possible for *Reynolds* and *Grashof* numbers ranging from 100 to 1000 and from 0 to 10, respectively. Yang (2002) proposed an oscillating bar as a vortex generator in a channel with heated obstacles. His results indicated that the vortices induced by the oscillating bar allowed an increase in heat transfer from the heated obstacles. Kim and Anand (2001) looked at the effect of using a slot behind each of six heated blocks on heat transfer from these blocks. Their results showed an enhancement factor ranging from 4.2 to 27.2 depending of slot size and *Reynolds* number. In a recent study, Korichi and Oufer (2005a,b) carried out a numerical investigation of the flow field and heat transfer enhancement in a channel containing three obstacles, two attached to the lower wall and one to the upper wall. The results showed that transition from steady to unsteady flow occurs at lower values of *Reynolds* number when compared to the channel with obstacles attached only to the lower wall. For instance, for the same obstacle dimensions and spacing value of 0.25, the value of Re_{cr} was found to be about 460. Moreover, the study showed that heat transfer was enhanced particularly for the second obstacle.

Except those reported by the present authors (2005a,b), all of the previously cited works are, in the best of our knowledge, concerned only with heat transfer in channels with heated blocks periodically attached to one single wall. The main objective here is to carry on with the investigation of the influence of alternating blocks between the upper and the lower walls of a channel. Special attention will be given to the analysis of flow evolution and heat transfer enhancement in the intermediate and low *Reynolds* number range without recourse to turbulent flow. Conduction heat transfer mode will also be considered.

2. Mathematical formulation

Fig. 1 shows the physical geometry considered in this study. It consists of a two dimensional horizontal channel containing heating blocks regularly distributed on both its lower and upper adiabatic walls. Each block base is maintained at a constant temperature. The flow is assumed to be laminar and incompressible, the fluid viscous Newtonian and buoyancy induced effects negligible. All the physical properties of the fluid and of the solid are considered constant. Buoyancy effects are neglected with respect to the forced convection effects because of the low temperature difference assumed. The *Prandtl* number is taken equal to 0.71. The dimensionless groups defined in the nomenclature are used to express the governing transport time-dependent equations in the dimensionless form. The resulting non-dimensional equations for mass, momentum and energy conservation are presented in the Cartesian coordinate system as follows:

Mass:

$$\frac{\partial u}{\partial x}+\frac{\partial v}{\partial y}=0 \tag{1}$$

X-momentum:

$$\frac{\partial u}{\partial \tau}+u\frac{\partial u}{\partial x}+v\frac{\partial u}{\partial y}=-\frac{\partial p}{\partial x}+\frac{1}{Re}\left(\frac{\partial^2 u}{\partial x^2}+\frac{\partial^2 u}{\partial y^2}\right) \tag{2}$$

Y-momentum:

$$\frac{\partial v}{\partial \tau}+u\frac{\partial v}{\partial x}+v\frac{\partial v}{\partial y}=-\frac{\partial p}{\partial y}+\frac{1}{Re}\left(\frac{\partial^2 v}{\partial x^2}+\frac{\partial^2 v}{\partial y^2}\right) \tag{3}$$

Energy:

For the fluid phase:

$$\frac{\partial \theta_f}{\partial \tau}+u\frac{\partial \theta_f}{\partial x}+v\frac{\partial \theta_f}{\partial y}=\frac{1}{Pe}\left(\frac{\partial^2 \theta_f}{\partial x^2}+\frac{\partial^2 \theta_f}{\partial y^2}\right) \tag{4}$$

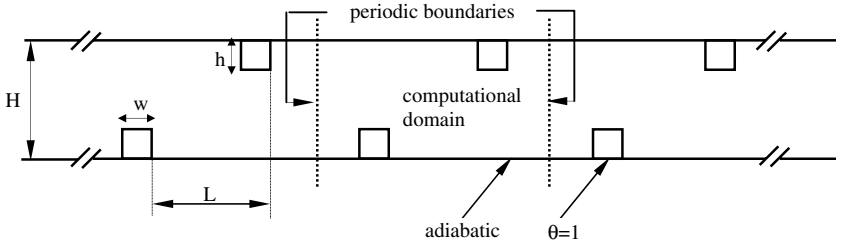

Fig. 1. Schematic diagram of computational domain and boundary conditions.

For the solid phase:

$$\frac{\partial \theta_s}{\partial \tau} = \alpha_s \left(\frac{\partial^2 \theta_s}{\partial x^2} + \frac{\partial^2 \theta_s}{\partial y^2} \right) \tag{5}$$

The non-dimensional variables are defined as follows:

$$u = \frac{u^*}{u_0}, \quad v = \frac{v^*}{u_0}, \quad x = \frac{x^*}{H}, \quad y = \frac{y^*}{H}, \quad \tau = t u_{0m}/H$$

$$p = \frac{p^*}{\rho u_{0m}^2}, \quad \theta = \frac{T - T_0}{T_w - T_0}; \quad Re = \frac{\rho u_{0m} H}{\mu};$$

$$Pe = Re \cdot Pr \quad \text{and} \quad \alpha = \frac{k}{\rho C_p}, \tag{6}$$

where u^*, v^* are the velocity components, p^* the pressure, T the temperature, H the channel height, u_{0m} the mean velocity at the inlet conditions, k_f the fluid thermal conductivity and α_s is the thermal diffusivity of the solid phase.

2.1. Boundary conditions

The geometry is periodic in the streamwise direction. Hence, only one module of the actual channel will be considered as suggested by Patankar et al. (1977). The flow field is assumed to be periodically fully developed which will allow the use of periodic boundary conditions in the streamwise direction. The temperature and pressure fields contain a non-periodic contribution but with a constant gradient. These two quantities may be decomposed into two parts: a periodic term and a linear varying term (in the periodic direction). More details on the periodic boundary conditions may be found elsewhere for imposed heat flux (Patankar et al., 1977). For imposed wall temperature, the same method was modified and then used at least in two different studies (Adachi and Uehara, 2001; Valencia et al., 2001). The dimensionless velocity components, temperature and pressure are such that:

$$u(x + L, y, t) = u(x, y, t); \quad v(x + L, y, t) = v(x, y, t) \tag{7}$$

$$\frac{\theta(x + L, y, t) - \theta_w}{\theta_b(x + L) - \theta_w} = \frac{\theta(x, x, t) - \theta_w}{\theta_b(x) - \theta_w} \tag{8}$$

where $\theta_b(X)$ is the cross-sectional local bulk temperature defined by

$$\theta_b(x) = \frac{\int_0^H |u| \theta \, dy}{\int_0^H |u| dy} \tag{9}$$

$$P(x + L, y, t) = P(x, y, t) + \beta \tag{10}$$

where $\beta = \beta(t)$ is the linearly varying component of the dimensionless pressure which results in a force acting on the fluid in the momentum equations and is adjusted every time step to satisfy the fixed mass flow rate condition.

At the channel walls ($y = 0$, $y = 1$), the no-slip condition is assumed, that is $u = v = 0$. As for the thermal boundary conditions, the walls are assumed to be insulated except at the obstacle bases where a constant temperature is imposed ($\theta = 1$). At the solid–fluid interface, continuity of both heat flux and temperature is also supposed to hold.

3. Numerical solution

The governing transport equations associated with the boundary conditions are solved using the finite volume formulation. The SIMPLER algorithm developed by Patankar (1980) is adopted. The time discretization scheme is implicit with second order accuracy. For the spatial discretization, the central second order differencing scheme is used for the diffusive terms and the QUICK scheme is used for the convective terms. The iterative solution is continued until the residuals for all computational cells become less than 10^{-6} for all dependent variables. Calculation is continued until both the velocity components and the temperature at the centerline ($x = 0.5$, $y = 1$) and at the module exit ($x = 0.5$, $y = 2$) become independent of time for the steady state or periodic in time for the self-sustained oscillatory flow.

For all calculations performed, a fine grid of 400×200 control volume was found to be sufficient for the range of *Reynolds* numbers investigated. The equally spaced grid system is used because the onset travelling waves engender moving high pressure and velocity gradients in the computational domain. Moreover, the displacement of these waves over the coarsed mesh results in higher calculation errors in this zone. In order to check grid independence, numerical simulations of the unsteady problem are performed with various grid sizes. For the three 200×100, 400×200 and 600×300 grid sizes and for $Re = 500$ and 1000, it is found that the maximum relative error for global parameters such as *Nusselt* number is only 3%. In order to show grid independence in the time domain, Fig. 2 presents the time-evolution of the u-velocity component for the three grid sizes and for $Re = 1000$. Furthermore, the maximum relative error in the u-velocity component profile at the centerline and exit sections is less than 2%. The time marching calculations are started with the fluid at rest and a small dimensionless time step $\Delta\tau = 0.001$ is considered in order

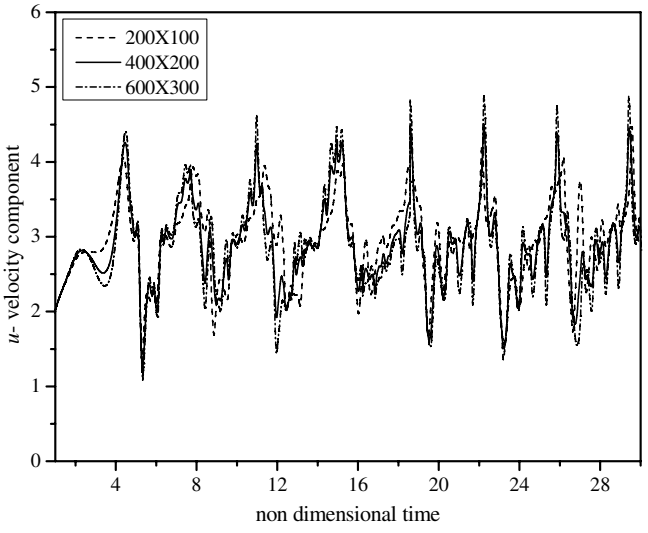

Fig. 2. Plot showing grid independence of velocity in time.

to capture the complex unsteady flow. Finally and in order to take into account the conjugate heat transfer, the treatment of the sudden changes of the thermophysical properties at the solid–fluid interface is handled by applying the domain extension method the details of which are presented by Chen and Han (2000). The code was already validated and used in previous works (Korichi et al., 2003; Korichi and Oufer, 2005a,b). It is important to note that 80,000 time steps are needed to obtain fully developed time periodic flow at $Re = 1000$ which takes about 60 h on a PC with P IV processor. However, it has to be noted that the development of the thermal field takes even more time.

4. Results and discussion

The dimensionless parameters to be considered and which characterize the flow field and heat transfer are as follows: The *Reynolds* number based on channel height is taken equal to 50, 500 and 1000, the obstacle dimensions (h, w) and the obstacle streamwise spacing (L) are taken as $h = w = 0.25$ and $L = 1$. At last, the solid to fluid thermal conductivity ratio is taken equal to 10.

In order to better take advantage of the obtained results, the following definitions are to be specified:

Local *Nusselt* number defined by the local temperature gradient at the wall:

$$Nu_x = -\left.\frac{\partial\theta}{\partial n}\right|_{\text{block surface}} \tag{11}$$

where n denotes normal to the solid surface and the temperature gradient at the wall is calculated using a three-point finite difference.

Time-averaged local *Nusselt* number by period:

$$\overline{Nu_X} = \frac{1}{\tau_p}\int_0^{\tau_p} Nu_X \,\mathrm{d}\tau \tag{12}$$

Mean face *Nusselt* number:

$$Nu_{\text{face}} = \frac{1}{A_i}\int_{A_i} Nu_X \,\mathrm{d}X \tag{13}$$

where A_i is the exposed face area.
Time-averaged face *Nusselt* number:

$$\overline{Nu_{\text{face}}} = \frac{1}{\tau_p}\int_0^{\tau_p} Nu_{\text{face}} \,\mathrm{d}\tau \tag{14}$$

Overall obstacle *Nusselt* number:

$$Nu_{\text{overall}} = \frac{\sum_{\text{face 1}}^{\text{face 3}} A_i Nu_i}{A_{\text{face 1}} + A_{\text{face 2}} + A_{\text{face 3}}} \tag{15}$$

Time-averaged overall *Nusselt* number around a heated obstacle:

$$\overline{Nu_{\text{overall}}} = \frac{1}{\tau_p}\int_0^{\tau_p} Nu_{\text{overall}} \,\mathrm{d}\tau \tag{16}$$

Global conjugate heat transfer in complex geometries such as electronic systems is strongly dependent on the local flow structure and relies therefore on the prediction of the local flow pattern. In such systems, the low velocities and small length scales correspond to low *Reynolds* number, hence leading to laminar flow characterized by complex structures such as separation, reattachment and recirculation. This makes an accurate determination of the distribution of the local convective heat transfer a difficult task. The following section is devoted to understanding the flow behaviour before analysis of heat transfer is undertaken.

4.1. Flow field

At low *Reynolds* number, the flow reaches steady state after an elapsed time which corresponds to the flow development time. The time history of the u-velocity component at the reference point $(x = 1, y = 0.5)$ for $Re = 50$ is plotted in Fig. 3 which indicates an exponential profile in the amplitude leading to an asymptotic value after a dimensionless time value of about 2. For the same steady state

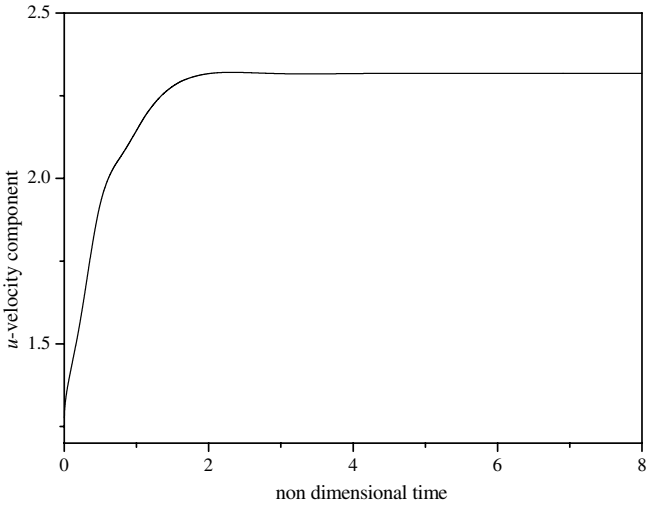

Fig. 3. u-velocity component history at the reference point $(x = 1, y = 0.5)$ for $Re = 50$.

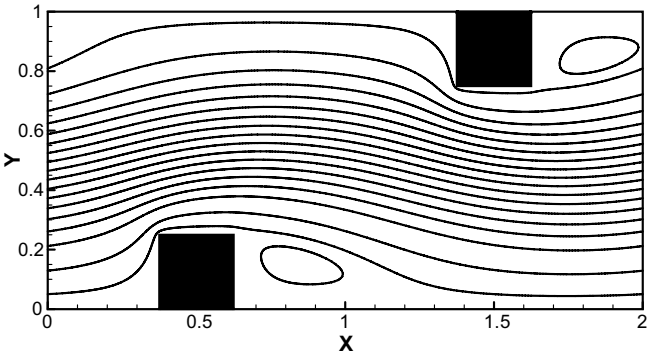

Fig. 4. Streamlines pattern for $Re = 50$.

case ($Re = 50$), the streamlines pattern in the computational domain is represented in Fig. 4. Due to the sudden lateral contraction, the flow deflects at the upstream corner of the lower obstacle. As the flow is accelerated and redirected toward the by pass region, a very small vortex is formed in the vicinity of the lower left corner. Downstream and as a result of the sudden expansion in the cross-section, the flow separates at the leading obstacle tip and a larger clockwise vortex is formed behind the same obstacle and flow reattachment is then established. The reattachment length is about 3.05 times the obstacle height. A similar phenomenon is observed near the obstacle mounted on the upper wall with counterclockwise vortices at the upstream and downstream obstacle. It is clear that the flow reattachment is established on the same wall before reaching the next obstacle situated downstream as opposed to the case of obstacles mounted periodically on one wall (Fu and Tong, 2004; Adachi and Uehara, 2001; Young and Vafai, 1998). In that case the production of inter-obstacles vortices is similar to the classic driven cavity flow in which vortices prevent the outer flow from reattaching to the channel wall. The use of obstacles in both upper and lower walls leads therefore to more interaction between the fluid and the solid surface.

As the *Reynolds* number increases, streamwise periodic contraction–expansion of the cross-section induces bifurcation from steady to unsteady state flow with the unsteadiness being more pronounced at higher *Reynolds* number. The transition from steady to unsteady flow occurs at lower *Reynolds* number values when compared to the case of channel with mounted obstacles on a single wall. The present study being not concerned with the determination of the critical *Reynolds* number, the results showed that the unsteady state is a time periodic self-sustained oscillatory flow. To illustrate such periodic structure, the time evolution of the u-velocity component at reference point ($x = 2$, $y = 0.5$) is presented in Fig. 5 for $Re = 1000$. It is noticed that the u-velocity component converges asymptotically to a periodic state after a long elapsed time. The dimensionless time period length τ_p is about 3.6 units. For clarity purposes, only the fully time periodic state is presented here.

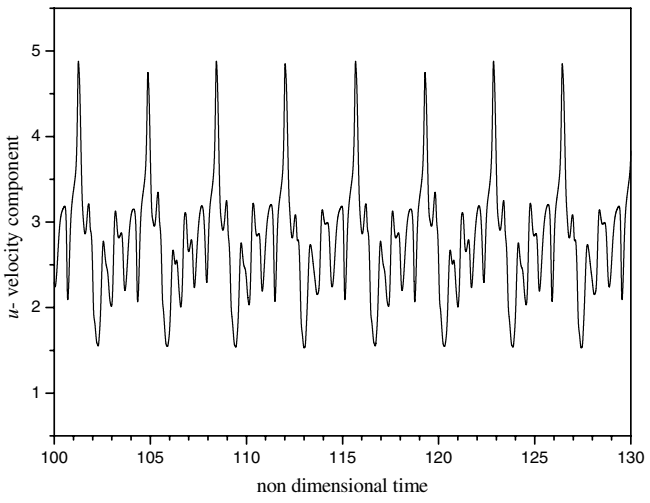

Fig. 5. Time history of the u-velocity component at the reference point ($x = 2.0$, $y = 0.5$) for $Re = 1000$.

In order to better understand the time periodic state and to allow satisfactory explanation for the flow structure in the entire computational domain, a full sequence of streamlines obtained at five time steps within one period of oscillation is represented in Fig. 6. Starting with Fig. 6a and as the lower block is approached, the flow deflects at the upstream corner to the bypass region. A jet-like flow then reaches the base and the frontal face of the upper obstacle. A small vortex is formed behind each obstacle and an even larger one is formed downstream both upper and lower obstacles. Each large vortex develops in time and moves downstream while the flow deflects near the obstacle which causes growth of the small vortex. The latter then moves with increasing strength pushing away the larger one as illustrated in Fig. 6b. A new small vortex is hence generated behind the obstacle which in turn moves downstream (Fig. 6c). The first large vortex coming from the upstream periodic module approaches the obstacle and moves upward passing over the obstacle. A new small vortex is formed upstream quite close to the obstacle base (Fig. 6d). Next, the vortex keeps growing until an entire cycle is completed (Fig. 6e). Each peak value appearing in the u-velocity component of Fig. 3 actually corresponds to the passage of the core flow near the reference point as illustrated in Fig. 6b. However, the lower negative value corresponds to the passage of the limit of the large vortex near the same point as clearly shown by Fig. 6d. It should be noted that a similar phenomenon takes place upstream and downstream the obstacle attached to the upper wall after a half period delay time and with counter-rotating vortices. These wave structures are characteristic of the Tollmien–Schlichting waves in the main channel, activated by the Kelvin–Helmohltz instabilities of the free shear layer spanning the interobstacle grooves.

It is important to mention that the fluid exchange between the interobstacle grooves and the main channel flow is due to unsteady vortical motion. Such fluid exchange occurs mainly because of the evolution in the v-velocity component causing fluid particles to be ejected toward the bulk flow as a result of fluid oscillation.

4.2. Heat transfer

An example of the obtained steady state thermal field is represented in Fig. 7 in which the isotherms contours are plotted for Re=50. It can be seen that close to the lower left obstacle corner, the isotherms are spread upstream due to the recirculation zone which negatively affects heat transfer. On the other hand and near the top left corner of the same obstacle, the isotherms are crowded by the core flow hence resulting in maximum heat transfer. Near the right upper corner of the obstacle, the isotherms contours are

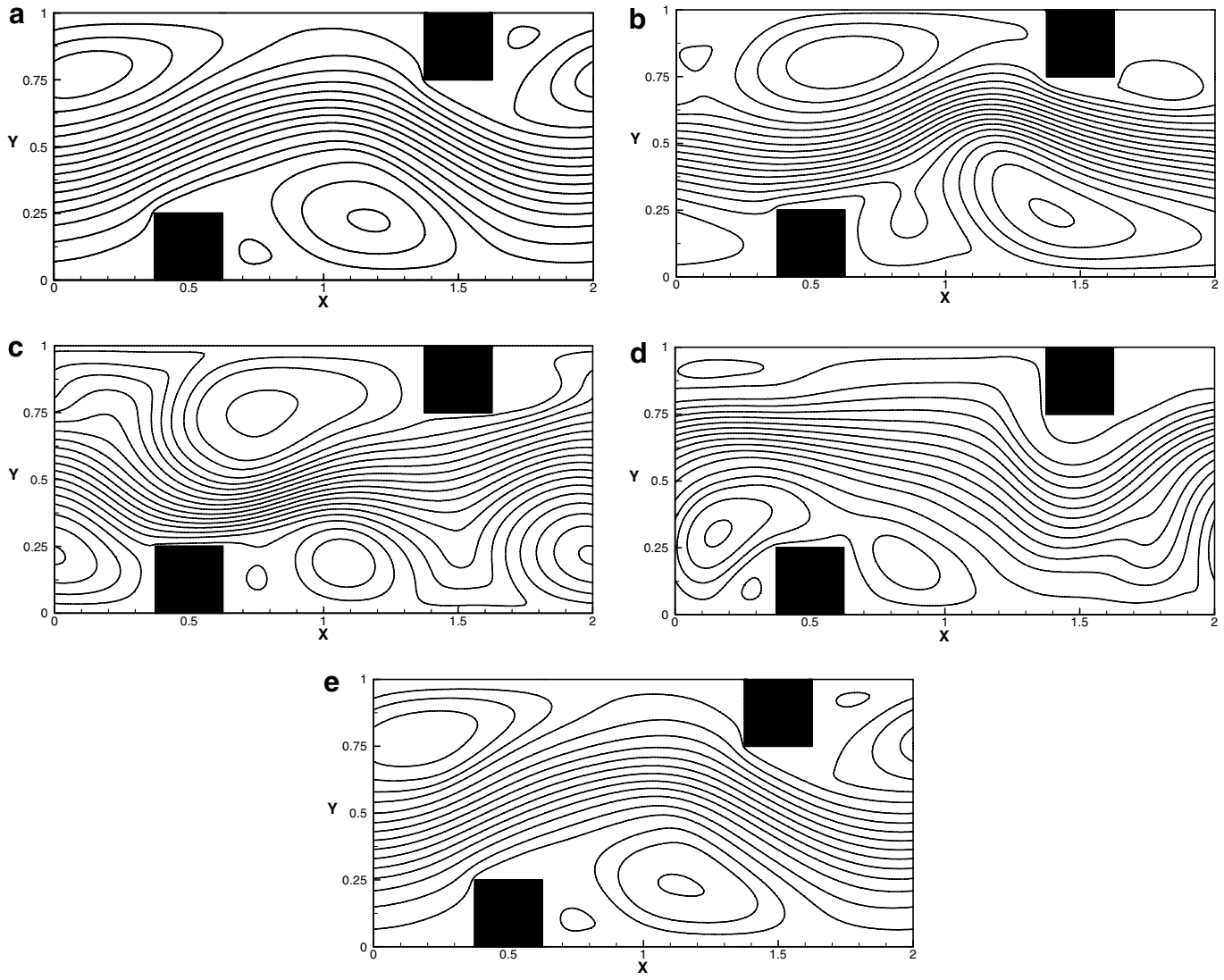

Fig. 6. Streamlines for five time steps of period of oscillation: (a) $\tau = 110.720$, (b) $\tau = 112.016$, (c) $\tau = 112.524$, (d) $\tau = 113.028$, (e) $\tau = 113.32$.

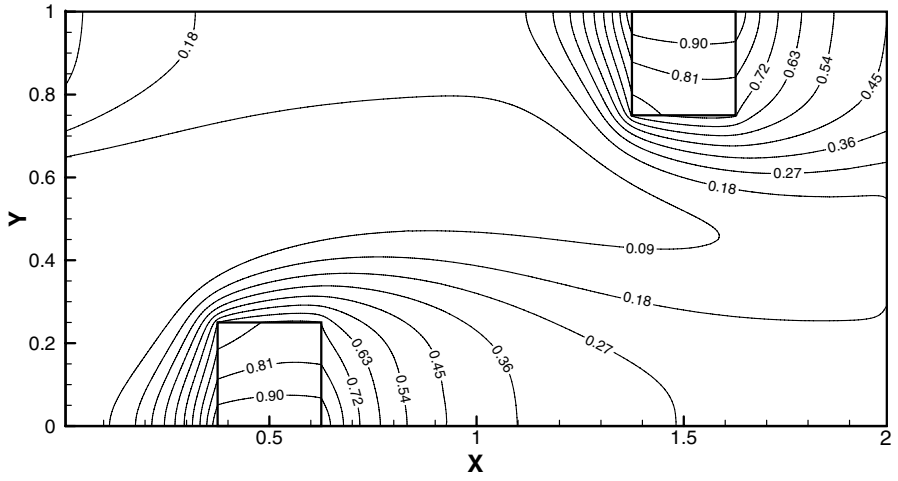

Fig. 7. Isotherms contours at steady state for $Re = 50$.

denser than for a channel with obstacles mounted on one wall as reported by Young and Vafai (1998). In such a geometry, the warm fluid is trapped in the slow recirculating flow within the grooves where diffusion is the dominant heat transfer mechanism through the free shear layer spanning the groove. Moreover, it was also previously shown that along a grooved channel heat transfer can be low due to this inefficient grooved region (Herman and Kang, 2000; Young and Vafai, 1998).

Fig. 8 shows the local *Nusselt* number evolution along the peripheral obstacle distance for both the upper and lower obstacles and for Re=50. The first general observation to be made is that heat transfer between the fluid and the lower obstacle is somewhat better than that with the upper obstacle with the difference being almost negligible toward the rear faces of the obstacles. Such differences may be explained by the fact that the fluid bulk temperature slightly increases as the fluid goes past the lower obstacle hence gaining some heat before it goes past the upper obstacle. Moreover, the rear faces of both the upper and lower blocks are in contact with fluids located in recirculating zones. Such zones are characterized by a weak mass exchange with the main flow and by some heat accumulation which may lead to closer main fluid temperatures in the vicinity of the blocks at the given *Reynolds* number value. Now, starting from the initial corner of each obstacle, *Nu* decreases along the frontal face to reach a minimum at a height value equal to 0.105 located between the flow reattachment coordinate and the recirculation zone limit. The value of *Nu* then increases quite sharply along the same frontal faces until peak values are attained at the second corner of each obstacle. Along the horizontal faces, *Nu* decreases sharply until we get very close to the downstream corner where it starts re-increasing to reach another peak of much less extent than that at 0.25 peripheral distance. Finally and along the right faces, the *Nusselt* number falls considerably below that observed for the other faces with however, positive values as opposed to the cavity driven flow (Young and Vafai, 1998). At the steady state flow, the diffusive heat transfer mode is non negligible compared to the convective mode toward the end of the last obstacle face. It is also observed that maximum heat transfer is obtained at the left outer corner of each obstacle.

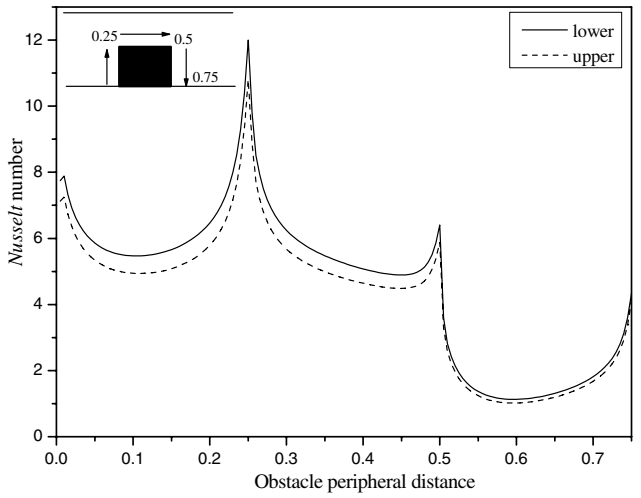

Fig. 8. Evolution of the local *Nusselt* number along obstacle peripheral distance for $Re = 50$.

For the time periodic oscillatory flow, only the time-averaged temperature and *Nusselt* number are considered in this study. As an example of the thermal field obtained in unsteady state, Fig. 9 shows the isotherms contours for $Re = 1000$. The temperature gradient near the obstacle solid walls is seen to become more intense except for a minor region situated in the vicinity of the base corners. The travelling waves tend to cause a periodic local compression–expansion of the thermal boundary layer on the heated block faces. In unsteady oscillatory flow, the thermal boundary layer is compressed progressively in time and the moving wave of vortex shedding interrupts continually the thermal boundary layer from a surface portion to

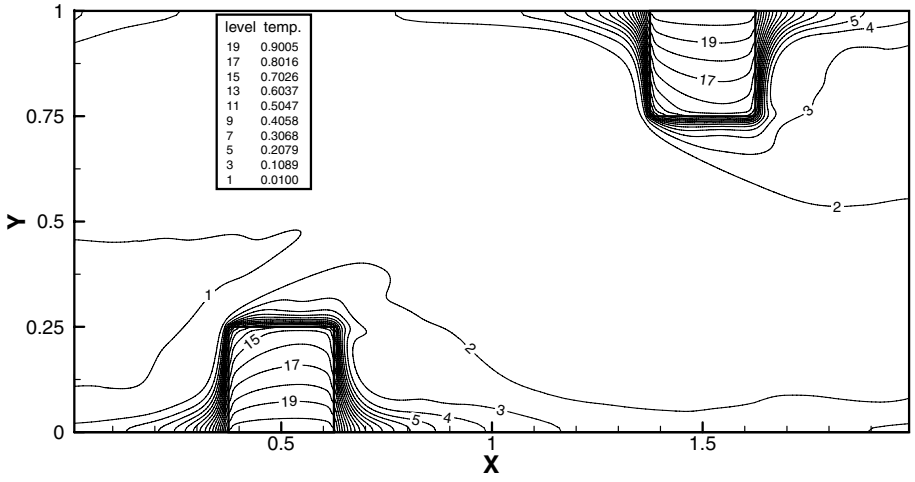

Fig. 9. Time averaged isotherms contours for $Re = 1000$.

another for the three exposed faces. A decrease in the thermal boundary layer thickness accompanied by the moving waves lead continually to an increase in the temperature gradient and hence in the heat transfer rate. The main result to be pointed out here is that the use of obstacles on both upper and lower channel walls makes the heat transfer obtained on the right obstacle faces not negligible and may therefore contribute to enhancement of the global heat transfer exchange.

Fig. 10 shows evolution of the time-averaged local *Nusselt* number along the obstacle peripheral distance for $Re = 500$ (a) and for $Re = 1000$ (b). The effect of unsteadiness on heat transfer is quite evident since the difference in heat transfer observed between the upper and lower obstacles for $Re = 500$ almost vanishes at $Re = 1000$. Another important observation is that the maximum heat transfer is still obtained at the left corner of the horizontal faces with a rather different evolution in the value of *Nu* all around the two obstacles. The effect of *Re* on heat transfer is further demonstrated in Fig. 11 where the time-averaged

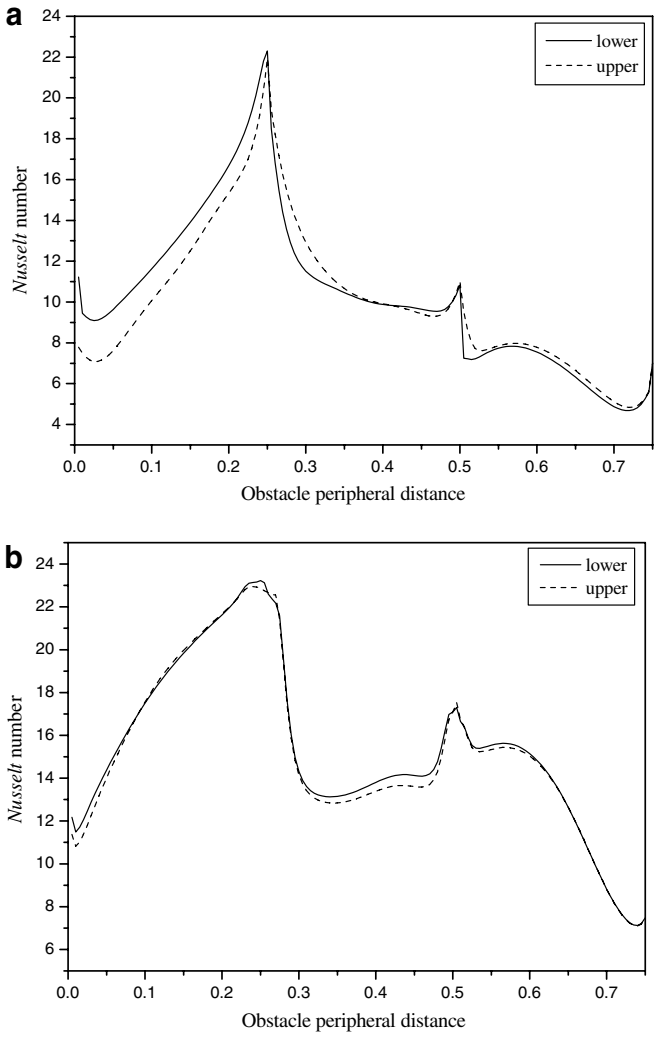

Fig. 10. Evolution of the time-averaged local *Nusselt* number along obstacle peripheral distance for (a) $Re = 500$, (b) $Re = 1000$.

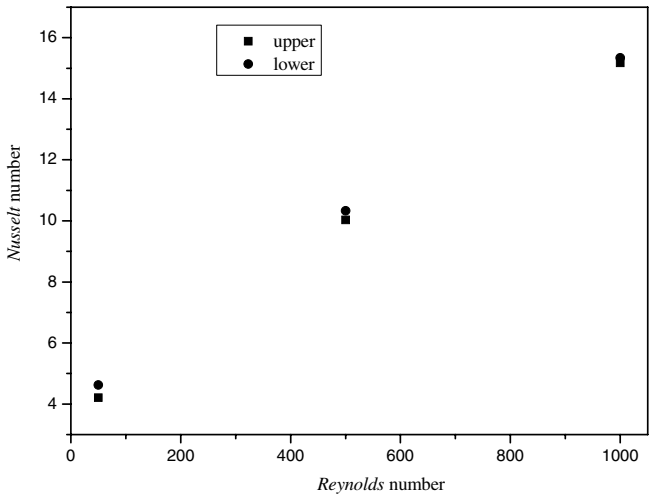

Fig. 11. Variation of the time-averaged overall *Nusselt* number with *Reynolds* number.

overall *Nusselt* number around the whole external surface of each obstacle is plotted against *Re* for the whole range investigated. Again, it appears clear that increasing *Re* leads to better heat transfer. For instance, increasing *Re* from 50 to 500 and from 500 to 1000 leads to 123.1% and 48.5% increase in *Nu*, respectively.

Finally, a comparison of heat transfer is made in terms of time-averaged overall *Nusselt* number between the case of channel with periodically mounted obstacles on its lower wall only and the present configuration. For instance, comparing the present results with those obtained by Young and Vafai (1998) for the fourth obstacle for which the flow was found to be periodic and fully developed showed up to 141% higher values in *Nu* at $Re = 1000$ when upper obstacles are present. Such interesting results suggest that much better cooling of electronic components may be obtained if similar configurations are adopted (in personal computers for example). The travelling waves in the grooved channel parts developed near both upper and lower walls do offer a major contribution to heat transfer. Such enhancement is mainly caused by the improvement of lateral mixing which disrupts the shear layer separating the bulk flow and the recirculating flow in the interobstacle groove. Introduction of vertical velocity components in this region also contributes to improving the fluid impact in particular with the vertical faces in the vicinity of which a hot fluid is mixed with the colder bulk fluid. The development of self-sustained oscillations leads therefore to heat transfer enhancement without the need to apply active external forces.

The heat transfer enhancement induced by the presence of blocks disposed in a staggered configuration between the upper and lower channel wall is unfortunately accompanied by rather important pressure losses. For instance, the 141% increase in *Nusselt* number cited previously is accompanied by an increase in the friction factor by a factor of about 19 which is a quite serious drawback, indeed. The reason for such large pressure drops is the important flow blockage and distortion caused by the presence of

the blocks. These distortions are believed to be mainly responsible for heat transfer enhancement between the fluid and the obstacle faces.

5. Conclusion

Numerical simulations of fluid flow and heat transfer in a horizontal channel with periodically mounted obstacles on both upper and lower walls were performed for $50 \leqslant Re \leqslant 1000$. The flow was found to be steady and stable in time at low enough *Reynolds* number values. However, as *Re* increased streamwise periodic contraction–expansion of the cross-section induced bifurcation to self-sustained oscillatory flow and led to onset of the Tollmien–Schlichting waves. The effect of such waves is to continually interrupt the thermal boundary layer in the obstacle vicinity and hence favors fluid exchange between the interobstacle grooves and the main channel flow. Significant heat transfer enhancement between the fluid and the heated obstacles of up to 123.1% and 48.5% in the overall *Nusselt* number was obtained when increasing *Re* from 50 to 500 and from 500 to 1000, respectively. When increasing *Reynolds* number, unsteadiness was found to be more pronounced resulting in increased heat transfer rates. A comparison with the results obtained in the literature for obstacles mounted only on one single wall showed that much higher values of up to 141% in *Nu* may be attained when obstacles are attached to both walls as is the case in the present work.

References

Adachi, T., Uehara, H., 2001. Correlation between heat transfer and pressure drop in channels with periodically grooved parts. International Journal of Heat and Mass Transfer 44 (22), 4333–4343.

Bilen, K., Yapici, S., 2001. Heat transfer from a surface fitted with rectangular blocks at different orientation angle. Heat and Mass Transfer 38 (7–8), 649–655.

Bilen, K., Akyol, U., Yapici, S., 2001. Heat transfer and friction correlations and thermal performance analysis for finned surfaces. Energy Conversion & Management 42 (9), 1071–1083.

Chen, X., Han, P., 2000. A note on the solution of conjugate heat transfer problems using SIMPLE-like algorithms. International Journal of Heat and Fluid Flow 21 (4), 463–467.

Fu, W.-S., Tong, B.-H., 2004. Numerical investigation of heat transfer characteristics of the heated blocks in the channel with a transversely oscillating cylinder. International Journal of Heat and Mass Transfer 47 (2), 341–351.

Garimella, S.V., Eibeck, P.A., 1990. Heat transfer characteristics of an array of protruding elements in single phase forced convection. International Journal of Heat and Mass Transfer 33 (12), 2659–2669.

Herman, C., Kang, E., 2000. Heat transfer enhancement in a grooved channel with curved vanes. International Journal of Heat and Mass Transfer 45 (18), 3741–3757.

Jurban, B.A., Swiety, S.A., Hamdan, M.A., 1996. Convective heat transfer and pressure drop characteristics of various array configurations to simulate the cooling of electronic modules. International Journal of Heat and Mass Transfer 39 (16), 3519–3529.

Kim, S.H., Anand, N.K., 2001. Use of slots to enhance forced convective cooling between channels with surface-mounted heat sources. Numerical Heat Transfer Part A 38 (1), 1–21.

Ko, K.-H., Anand, N.K., 2003. Use of porous baffles to enhance heat transfer in a rectangular channel. International Journal of Heat and Mass Transfer 46 (22), 4191–4199.

Korichi, A., Oufer, L., 2005a. Numerical heat transfer in a rectangular channel with mounted obstacles on the upper and lower walls. International Journal of Thermal Sciences 44, 644–655.

Korichi, A., Oufer, L., 2005b. Unsteady heat transfer and pressure drop in channels with upper and lower walls mounted obstacles. Numerical Heat Transfer Part A 48 (7), 711–729.

Korichi, A., Cherifi, H., Oufer, L., 2003. Etude numérique des transferts de chaleur par convection forcée dans un canal en présence d'obstacles chauffés. In Proceedings of the 11th International Heat Transfer Meeting JITH, Algiers, Algeria, 2003, pp. 211–219.

Leung, C.W., Chan, T.L., Probert, S.B., Kang, H.J., 1999. Forced convection from a horizontal ribbed rectangular base-plate penetrated by arrays of holes. Applied Energy 62 (2), 81–95.

Meinders, E.R., Hanjalic', K., 2002. Experimental heat transfer from in-line and staggered configurations of two wall-mounted cubes. International Journal of Heat and Mass Transfer 45 (3), 465–482.

Patankar, S.V., 1980. Numerical Heat Transfer and Fluid Flow. Hemisphere, New York.

Patankar, S.V., Liu, C.H., Sparrow, E.M., 1977. Fully developed flow and heat transfer in ducts having streamwise-periodic variations of cross-sectional area. ASME Journal of Heat Transfer 99, 180–186.

Sara, O.N., 2003. Performance analysis of rectangular ducts with staggered square pin fins. Energy Conversion & Management 44 (6), 1787–1803.

Sara, O.N., Pekdemir, T., Yapici, S., Ersahan, H., 2000. Thermal performance analysis for solid and perforated blocks on a flat surface in duct flow. Energy Conversion & Management 41 (10), 1019–1028.

Sara, O.N., Pekdemir, T., Yapici, S., Yilmaz, M., 2001a. Enhancement of heat transfer from a surface in a channel flow by attachment of blocks. Journal of Energy Research 25 (7), 563–576.

Sara, O.N., Pekdemir, T., Yapici, S., Yilmaz, M., 2001b. Heat transfer enhancement in a channel flow with perforated rectangular blocks. International Journal of Heat and Fluid Flow 22 (5), 509–518.

Sultan, G.I., 2000. Enhancing forced convection heat transfer from multiple protruding heat sources simulating electronic components in horizontal channel by passive cooling. Microelectronics Journal 31 (9–10), 773–779.

Tsay, Y.-L., Cheng, J.-C., Chang, T.-S., 2003. Enhancement of heat transfer from surface-mounted block heat sources in a duct with baffles. Numerical Heat Transfer Part A 43 (8), 827–841.

Valencia, A., Martin, J.S., Gormaz, R., 2001. Numerical study of unsteady flow and heat transfer in channels with periodically mounted square bars. Heat and Mass Transfer 37, 265–270.

Wu, H.W., Perng, S.W., 1999. Effect of oblique plate in heat transfer enhancement of mixed convection over heated blocks in horizontal channel. International Journal of Heat and Mass Transfer 42 (7), 1217–1235.

Yang, S.-J., 2002. A numerical investigation of heat transfer enhancement for electronic devices using an oscillating vortex generator. Numerical Heat Transfer Part A 42 (3), 269–284.

Young, T.J., Vafai, K., 1998. Convective flow and heat transfer in channel containing multiple heated obstacles. International Journal of Heat and Mass Transfer 41 (21), 3279–3298.